Effect of human passage on transport through an air curtain

Narsing K. Jha[1]† D. Frank[1] L. Darracq[2] P. F. Linden[1]

[1]Department of Applied Mathematics and Theoretical Physics, University of Cambridge, Wilberforce Road, CB3 0WA Cambridge, UK
[2]Department of Mechanical Engineering, Ecole Polytechnique, France

(Received 19 October 2018)

Air curtains are commonly used as separation barriers to reduce heat and mass fluxes across open doorways of a building. Although they enable the unhampered passage of humans and vehicles through doorways, the effect of this traffic on the stability and effectiveness of an air curtain is not well understood. As a model of human passage, we examine the effect of a vertical cylinder passing through an air curtain separating two zones at either equal or different temperatures and, therefore, at either the same or different densities. Small-scale laboratory experiments were performed using fresh water and aqueous salt and sugar solutions to establish the equivalent density differences across the doorway. Parameters and geometries for the experiments were chosen appropriately to maintain dynamical similarity to full-scale air curtain installations. We find that the sealing effectiveness and stability of an air curtain reduces with increasing cylinder speed. Visualisations of the curtain and the cylinder wake reveal that the infiltration of the fluid transported in the wake results from the disruption of the air curtain by the cylinder thereby reducing its effectiveness. The infiltration increases with cylinder speed due to the faster wake velocity and the longer time needed for the re-establishment of the curtain. We also observed that the reduction in effectiveness is independent of the direction of travel, i.e. from the warm side to the cold side or vice-versa, because the cylinder speed, and the equivalent human walking speed, is an order of magnitude faster than the typical buoyancy-driven exchange flow. We used time-resolved particle image velocimetry to study the interaction of the curtain and the cylinder wake. Despite the possibility of transport of air-borne contamination in a human wake, we conclude that an air curtain can be useful in protecting isolated hospital rooms for infectious and immunocompromised patients.

Key words:

1. Introduction

Air curtains, consisting of a planar air jet directed across a doorway, are used to reduce the heat and mass transfer across doorways separating two zones in a building at different temperatures or between the inside and outside of a building. The air curtain, usually directed vertically downwards from the top of the doorway, disrupts the buoyancy-driven exchange flow that results from the temperature difference, thereby reducing the exchange (Frank & Linden 2014). Such buoyancy-driven exchange flows are, for example, detrimental in industry and laboratory clean rooms where air infiltration between clean

† Email address for correspondence: navinnaru88@gmail.com

and dirty environments can contaminate processing. In hospitals, air infiltration between rooms can result in the spread of disease or cause extra complications for immunocompromised patients (Beggs 2003; Hoffman *et al.* 1999; Lowbury *et al.* 1971; Adams *et al.* 2011). Moreover, human and vehicular traffic through open doorways is also accompanied by additional transport of heat, along with many other undesirable substances such as moisture, air-borne contaminants, odours, insects and microorganisms in their wakes.

In practice, an air curtain is produced by a fan mounted in a manifold usually above the doorway, which drives air through vents in the manifold and thus establishes a downward flow of air that acts as a virtual barrier at the doorway. Compared to other separation methods such as vestibules, revolving doors or strip curtains, air curtains have reduced space requirements, are more hygienic and provide the least hindrance to the traffic. Under optimal operating conditions, an air curtain can reduce the air exchange by about 80% compared to an open doorway.

While turbulent jets are well understood (Rajaratnam 1976), their use as a separation barrier is still being explored. The first fundamental and systematic study on air curtains was carried out by Hayes & Stoecker (1969*a*,*b*). They identified the deflection modulus D_m, defined as the ratio of the jet momentum flux and the pressure difference due to the 'stack effect' associated with the buoyancy difference across the doorway,

$$D_m = \frac{(\rho_0 Q_0^2/b_0)}{gH^2\,(\rho_d - \rho_l)} = \frac{Q_0^2}{gb_0H^2\left(\frac{T_0}{T_d} - \frac{T_0}{T_l}\right)}, \tag{1.1}$$

as the key parameter for the performance of an air curtain. Here, ρ_0, T_0 and Q_0 are the density, temperature and discharge per unit nozzle length of the jet at the manifold exit, respectively. We approximate the details of this exit as a two-dimensional nozzle of width b_0. The height of the doorway is denoted by H and g is the acceleration due to the gravity. For a doorway between two zones with different temperatures the subscripts d and l are used to denote the properties of the dense (cold) and light (warm) air, respectively. The value of D_m determines the stability of an air curtain: a curtain is said to be stable if it reaches the opposite side of the doorway, i.e. the floor if directed downwards, and unstable otherwise.

The performance of an air curtain is quantified by the sealing effectiveness E, defined as the fraction of the exchange flow prevented by the air curtain compared to the open doorway condition,

$$E \equiv \frac{q - q_{ac}}{q}. \tag{1.2}$$

Here q_{ac} and q are the exchange flows through the doorway with and without the air curtain, respectively. A major aim of modelling air curtains is to determine the relationship between E and D_m. Typically, E increases with D_m as a result of disrupting the organised buoyancy-driven flow through the doorway, until a maximum value of E is reached. With further increase in D_m, E decreases. This degradation in performance at higher D_m is caused by mixing across the doorway produced by the air curtain itself (Frank & Linden 2014).

Examining the flow at high D_m, Guyonnaud *et al.* (2000) highlighted the importance of shear layer eddies in the jet and the jet impingement on the floor on the effectiveness E. Sirén (2003*a*,*b*) presented methods for dimensioning an air curtain using momentum and moment-of-momentum balance principles. He also determined the minimum momentum required for the air curtain to reach the opposite side of the doorway, both in the presence and absence of a wind. Sirén (2003*b*) focused on the thermal behavior of the air curtain deriving the expression for the thermal loss and comparing it with empirical results.

Full-scale experiments have been performed by Howell & Shibata (1980) and Foster *et al.* (2006), which showed satisfactory agreement with the theoretical predictions of Hayes & Stoecker (1969*b*). Numerical simulations (Costa *et al.* 2006; Foster 2007; Gonçalves *et al.* 2012), a semi-analytical model (Giráldez *et al.* 2013) and laboratory-scale studies in water (Frank & Linden 2014, 2015) are all in satisfactory agreement with full-scale tests on an air curtain in an otherwise sealed building.

Frank & Linden (2014) studied the effect of an additional ventilation pathway, such as an open window, on the effectiveness of an air curtain and modelled the observed change of performance of the air curtain caused by the resulting change in the neutral level. Frank & Linden (2015) investigated a heated air curtain and observed the reduced stability, effectiveness and energy efficiency of the curtain associated with the opposing buoyancy force. Additionally, wind and pressurised chambers provide external forcing to the air curtain and can destabilise the curtain causing severe oscillations (Havet *et al.* 2003; Rouaud & Havet 2006).

Choi & Edwards (2012) and Tang *et al.* (2013) studied the contaminant transport caused by humans walking through a doorway using large eddy simulation (LES) computations and laboratory experiments, respectively. They also considered the effect of opening various types of doors such as hinged or sliding, and found that the effect of the induced air movement on the human wake had a noticeable effect.

However, the interaction of humans and their wakes with an air curtain has not been studied and is the motivation for the present work. In this paper, we describe laboratory experiments designed to investigate the effect of human passage on the effectiveness and the stability of an air curtain. The paper is structured as follows. In §2, we describe the experiments and the techniques used for flow visualization and measurements of the effectiveness and the velocity field. The experimental results are presented in §3. In §3.1, we describe the effect of the human passage and the direction of travel on the effectiveness of an air curtain. We discuss the infiltrated wake volume with and without the air curtain in §3.2, and dye visualizations of the jet and the infiltration by the wake are described in §3.3. Velocity field measurements from particle image velocimetry (PIV) showing the interaction of the jet and the wake are presented in §3.4. Finally, in §4 we summarise our conclusions provide an overview of how the present study can be helpful for a better design of an air curtain, and discuss strategies for the reduction of the traffic effects on the air curtain effectiveness in practical conditions.

2. Experimental methods

The experiments were performed with fresh water and aqueous salt and sugar solutions in a tank with dimensions of length 2 m, width 0.2 m, and depth 0.25 m. The tank was divided in two equal compartments by a vertical gate, which represented a doorway in a corridor or in a building. One side of the tank was filled with water of density ρ_l and the other side with water of density ρ_d. The density ratio ρ_l/ρ_d was kept in the range $0.96-1$ to maintain the validity of the Boussinesq approximation. The air curtain device (ACD) consisted of a horizontal cylinder of length 195 mm, closed at the ends, which was fitted across the top of the tank. The cylinder was filled with fine sponge wrapped in a steel wire mesh to uniformly distribute the flow and supplied with fluid of density ρ_0 from an overhead tank. A sequence of 39, 1.0 mm diameter holes separated by 5.0 mm (centre to centre) was drilled along the length of the cylinder, facing downwards on the opposite side to the inlet connections. The circular water jets from the holes merged a few diameters downstream of the nozzle and formed a planar turbulent jet further

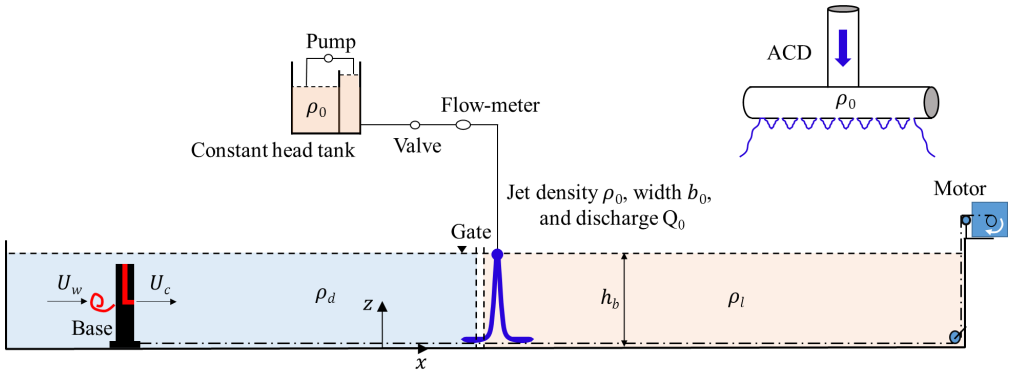

Figure 1: (Colour online) Schematic showing the experimental set-up. Experiments were conducted in a long rectangular tank, each half of which was filled with dense and light fluid of density ρ_d and ρ_l, respectively. Fluid of density ρ_0 was supplied to the air curtain device (ACD) from a constant head tank. A vertical gate was installed beside the curtain to separate the fluid when the air curtain device was switched off. The cylinder was driven by a motor, connected by a flexible thread and a system of pulleys. A dye port injecting red dye was attached to the cylinder to track the wake and the infiltration. Blue coloured dye was injected at the nozzle exit to visualise the air curtain.

downstream (Knystautas 1964). The effective planar nozzle width $b_0 = 0.157\,\text{mm}$, was determined as the ratio of total hole area and length of the cylinder.

The air curtain device was placed midway along the length the tank, with the holes on the underside of the cylinder just submerged, and was located near the gate position on the side of the tank with water of density ρ_l (figure 1). The flow rate, measured by the Omega flow meter (FLR1013), was maintained at a constant value of approximately $5\,\text{L}\,\text{min}^{-1}$, with an accuracy of $\pm 3\%$. The turbulence level at the nozzle exit was not measured but Guyonnaud *et al.* (2000) argued that the turbulence intensity does not noticeably affect the air curtain performance.

To represent the passage of a person through an air curtain a cylinder of diameter $d = 50\,\text{mm}$ and height $l = 170\,\text{mm}$ was pulled at a constant velocity U_c along the centreline of the tank. The base of the cylinder was pulled by a flexible line, attached to a motor via a series of pulleys. To ensure stability during its motion the base of the cylinder consisted of a disc with a larger diameter of 80 mm and height of 15 mm. The speed of the cylinder was controlled by the motor and could be varied in the range of $50 - 250\,\text{mm}\,\text{s}^{-1}$. The height and diameter of the cylinder were chosen to be representative of a typical adult when compared to the height and width of a typical doorway. The velocity of the cylinder was chosen to ensure that the cylinder motion was dynamically similar to human walking. The length of the experimental tank ensured there was an appropriate distance to establish the wake of the cylinder before and after its passage through the air curtain.

To facilitate flow visualisation, we used two dye ports injecting dye of two different colours. One dye injection point (blue dye) was placed just underneath the nozzle of the air curtain device on the centreline of the tank. The other dye port (red dye) was attached to the front of the cylinder at half the height of the cylinder. A Nikon D3300 camera was used to capture the top and the side-view videos of the experiments at 24 fps.

We conducted experiments for two different situations. For series A, the fluid of density ρ_l was fresh water and the fluid of density ρ_d was salt water. The supply to the air curtain

was also fresh water, so that in this scenario $\rho_0 = \rho_l < \rho_d$. This arrangement models the situation of a person entering a warm building from the cold outside environment. For series B, the fluid of density ρ_l as well as the initial air curtain supply was sugar water and the fluid of density ρ_d was salt water. For these experiments, we set the densities to be equal, $\rho_0 = \rho_l = \rho_d$, so that there is no buoyancy-driven flow across the doorway and, since molecular diffusion is unimportant in these experiments, the sugar and salt act as passive tracers. All densities were measured using an Anton-Paar density meter DMA 5000 with an accuracy of $7 \times 10^{-3}\,\mathrm{kg\,m^{-3}}$.

At the beginning of an experiment for series A, the dense fluid side ρ_d was filled with salt water up to the height of 210 mm. The water level in the fresh water side was initially set slightly below at 205 mm. The experiment was started by switching on the air curtain device. Once the flow in the jet reached a steady state and the water level in the fresh water side reached the same level as in the salt water side, the vertical barrier between the two compartments was opened and the blue dye port switched on. Subsequently, the cylinder was set into motion at a constant velocity U_c, and the red dye port was opened to visualise the cylinder wake. The motor driving the cylinder was stopped when the cylinder reached the opposite end of the tank and the vertical gate was immediately closed. We also immediately stopped the flow through the air curtain and closed all the dye ports. The total time during which the gate was open and allowed the exchange flow (about 10 s) was measured using a stop watch to a precision of 0.1 s. The liquid in the two compartments was fully mixed and the new densities were measured on the light and dense fluid sides, denoted as ρ_{ln} and ρ_{dn}, respectively. We investigated both directions of travel for the cylinder: from the salt water side (ρ_d) to the fresh water side (ρ_l) and vice-versa.

Using the mass conservation for the light fluid half (considering $\rho_0 = \rho_l$), the intruded volume V_i was calculated from the measured initial and final densities as $V_i = (V_l + \beta q_0 t)(\rho_{ln} - \rho_l)/(\rho_d - \rho_l)$, where q_0 is the total source volume flux of the air curtain, i.e. not per unit length, and V_l is the volume of the light-fluid half of the tank. We denote by β the fraction of the air curtain volume flux that spilled into the light-fluid compartment. For typical jet nozzle volume fluxes of $5\,\mathrm{L\,min^{-1}}$ and run-times of about 10 s for these experiments, the added volume of water by the curtain to the light fluid compartment was about 2% of the total volume if $\beta = 1$. Any value of β between 0.5 and 1 can be chosen with an error of less than 2% of V_i, and we used $\beta = 0.5$. We obtained the reference volume flux (q) by calculating theoretically the amount of exchanged fluid due to the intruding gravity current when the air curtain is switched off using the experimentally measured discharge coefficient C_d. The theoretical expression for the buoyancy-driven exchange, also known as the orifice equation, is written as $q = \frac{1}{3} C_d A \sqrt{g' H}$, where g' is the reduced gravity ($g' = g(1 - \frac{\rho_l}{\rho_d})$), A is the area of opening, and H is the height of opening. The measured discharge co-efficient for the present opening configuration was about 0.55, which is close to the 0.6 reported in the literature for sharp openings (Linden 1999). In this series of experiments, we varied the value of the deflection modulus D_m by changing the density ρ_d from $1002 - 1041\,\mathrm{kg\,m^{-3}}$.

For series B, we used the same experimental procedure, except that we replaced the fresh water by aqueous sugar solutions and adjusted the densities so that $\rho_0 = \rho_l = \rho_d = 1040 \pm 0.5\,\mathrm{kg\,m^{-3}}$. Here, the cylinder was dragged only from the salt water side (ρ_d) to the sugar water side (ρ_l) with and without the air curtain. We used a calibrated conductivity probe to measure the salt content in each half of the tank at the beginning and the end of an experiment. These values were then used to calculate the effect of the air curtain on the (passive) contaminant transport. The error in the entrained volume measurement is approximately $\pm 2.5\%$ at highest cylinder speed and $\pm 10\%$ at lowest cylinder speed.

The flow field was measured using time-resolved particle image velocimetry (PIV). As we shall see later, the dominant interaction takes place between the air curtain and the cylinder wake, since for typical temperature differences the buoyancy-driven flow through the doorway is significantly smaller than the cylinder wake velocity. Consequently, we restricted the use of PIV to cases with no density difference (pure water) to avoid the impact of refractive index changes. The velocity field was measured in the streamwise and vertical plane through the axis of the cylinder. A thin vertical light sheet was generated by passing the light from a pair of 300 W xenon arc lamps through a thin slit. The arc lamp is equipped with paraboloidal dichroic reflectors, which produce about 35 W of visible light. The light sheet entered the tank after being reflected from a cold mirror to avoid heating the perspex tank. The flow was seeded with 50 µm diameter particles, which were approximately neutrally buoyant. Particle concentrations were chosen such that each correlation box used in the PIV analysis had 6 to 8 particles to provide good correlations. Images were recorded using an ISVI camera with a full resolution of 12 Mpixel. A Nikon 85mm lens was used and images were captured at a frame rate of 400 f.p.s. with a resolution of 2048×2048 pixels. Exposure times were kept at 0.8 ms and no streaking of particles was observed. We performed the analysis of the image pairs in the DigiFlow software using a box size of 33×33 pixels. The present PIV measurements were similar to those described in more detail in Olsthoorn & Dalziel (2015).

In the following, we describe the results in terms of the nondimensional cylinder speed $U^* \equiv U_c/w_m$, where the mean velocity of jet front $w_m \equiv H/t_{fw}$ and t_{fw} is the time taken by the curtain to reach the opposite side from nozzle exit in the absence of any buoyancy effects. For a typical value of ACD flowrate $q_0 \sim 5\,\mathrm{L\,min^{-1}}$, w_m is about $400\,\mathrm{mm\,s^{-1}}$. We varied the cylinder speed from 62.5 to $210\,\mathrm{mm\,s^{-1}}$, which results in values of U^* from 0.16 to 0.52.

These values are typical for human passage through a full-scale air curtain. For example, walking at a moderate pace of $1\,\mathrm{m\,s^{-1}} = 3.6\,\mathrm{km\,h^{-1}}$ through a typical air curtain with speed $w_m \sim 2\,\mathrm{m\,s^{-1}}$, gives $U^* \sim 0.5$. As mentioned above, this walking speed is significantly faster than typical buoyancy-driven flow, e.g. a 10K temperature difference across a 2 m high doorway produces a gravity current with speed $\approx 0.15\,\mathrm{m\,s^{-1}}$, and so the direction of travel has little impact on the exchange. Finally, we note that the cylinder Reynolds numbers $Re \equiv U_c d/\nu$ are in the range 3,100 – 10,500 in our experiments compared with $\sim 50,000$ at full scale. However, given that the flow round the cylinder is separated and the jet is turbulent at the laboratory scale we expect this difference in Reynolds numbers not to be significant.

3. Results

3.1. *Effectiveness measurements*

The variation of the air curtain effectiveness with the deflection modulus for different cylinder speeds for series A is shown in figures 2(a) and (b) for the transits from the dense to the light fluid side and vice-versa, respectively. For the base case of the air curtain operating without the cylinder transit, the effectiveness E first increases with the deflection modulus until it reaches a maximum value of about 0.8 at $D_m \sim 0.2$, and then decreases slowly with further increase in D_m. This value of maximum effectiveness is similar to the previously observed value by Frank & Linden (2014) and others. At the maximum effectiveness, the curtain is stable and impinges on the floor. As mentioned previously, with further increase in D_m, the effectiveness E reduces because of the en-

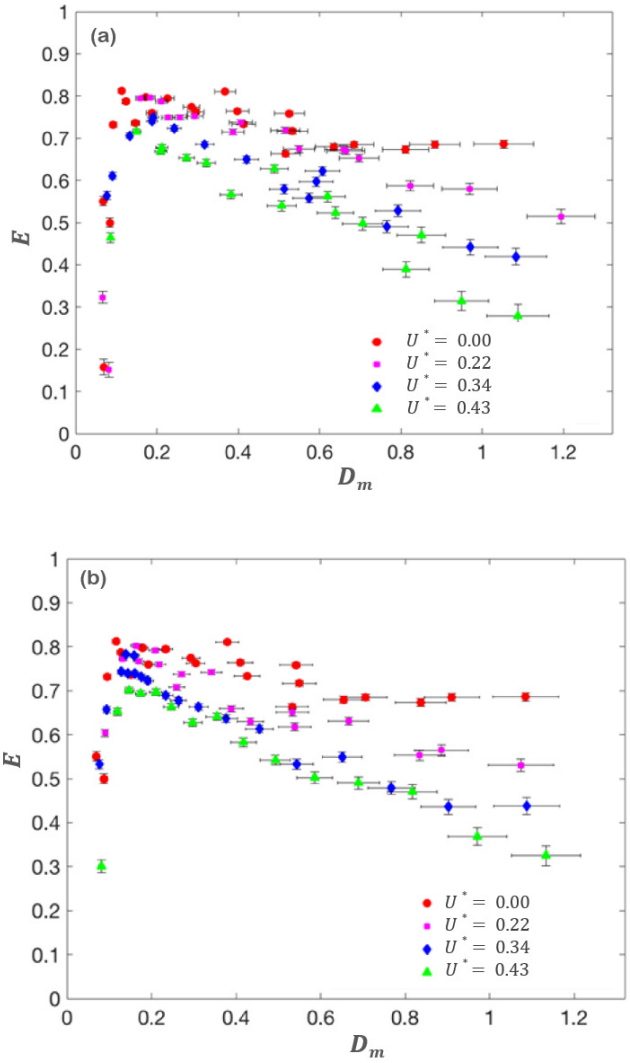

Figure 2: (Colour online) Air curtain effectiveness E as a function of the deflection modulus D_m for different dimensionless cylinder speeds $U^* \equiv U_c/w_m$. In (a) the cylinder moves from the dense fluid to the light fluid side while in (b) the motion is in the opposite direction. In these experiments the values of the deflection modulus D_m were changed by changing the density difference across the curtain – see (1.1). Consequently, the error bars reflect the uncertainty in the density difference during the course of an experiment.

hanced mixing between two compartments due to the jet entrainment and impingement at the bottom.

The dependence of the effectiveness E on D_m is shown in figure 2 for different values of the dimensionless cylinder speed ($U^* \equiv U_c/w_m$). In general, the effectiveness E was reduced by the passage of the cylinder and, for a given value of D_m, the reduction increased with increasing cylinder speed. At small values of the deflection modulus, $D_m \leq 0.15$, the air curtain is inherently unstable and, thus, the motion of the cylinder had

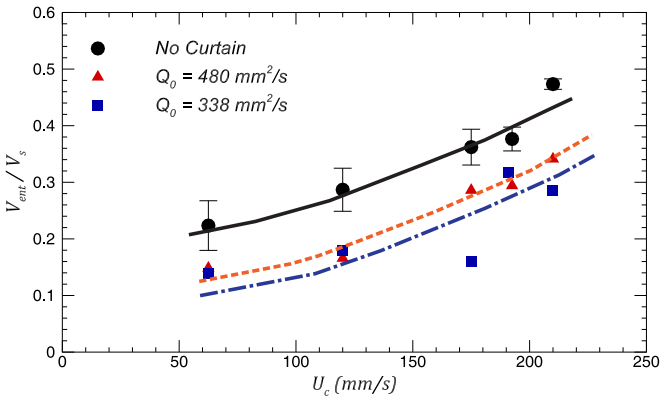

Figure 3: (Colour online) The volume V_{ent} of salt transported across the doorway between two isothermal spaces at different cylinder speeds (U_c), with and without the air curtain. Curves are shown to highlight the trend of the data and also to demarcate among different air curtain conditions.

no noticeable effect on the effectiveness. For deflection modulus $D_m \approx 0.2$ where the effectiveness is maximum, E was reduced by approximately 10% at the highest cylinder velocity. At higher values of the deflection modulus the reduction in E increased with increasing D_m. At $D_m > 1$ the effectiveness was reduced by about 25% compared to the base case for $U^* = 0.22$, and more than 55% for $U^* = 0.43$.

As discussed in § 2, in the present experiments the velocity of the buoyancy-driven flow across the doorway is significantly smaller than the cylinder speed.Consequently, we expect the direction of the cylinder motion not to play a role, and this is confirmed by the similarity in the data in figures 2(a) and (b).

The reduction of effectiveness with increasing cylinder speed reflects the additional transport across the curtain associated with the stronger wake at higher speeds. We examine this quantitatively in the subsection § 3.3.

3.2. *Cylinder passage between two isothermal rooms*

The series B experiments used aqueous sugar and salt solutions of the same density on either side of the curtain. Since the molecular diffusion coefficients of salt and sugar are similar and, more importantly, small, the solutes acted as passive tracers. The cylinder started on the saline side so that the amount of salt on the sugar side at the end of the experiment was a result of transport in the wake of the cylinder and the impact of the air curtain. From measurements of the salt concentration we calculated the volume V_{ent} transported across the doorway. We nondimensionalise V_{ent} by the swept volume of the cylinder $V_s = U_w l d \Delta t$, which is the volume that can pass through the doorway in the absence of curtain, where U_w is the average speed of flow in the wake and Δt is one half the duration of the transit time from one end of the tank to the other end. It is further assumed that $U_w \approx U_c$ in which case $V_s = ldL$, where L is the swept length of the cylinder or half length of channel. The results are shown in figure 3 for the case of no air curtain and for two curtain strengths of $Q_0 = 480$ and $338\,\mathrm{mm\,s^{-2}}$.

We observed, as expected, that the transport across the doorway increased with increasing cylinder speed. The increase comparable for all three cases and is slightly greater than linear in U_c. We also see that the air curtain reduced the volume transport up to about 50%. In the absence of buoyancy forces the curtain always reached the floor of the

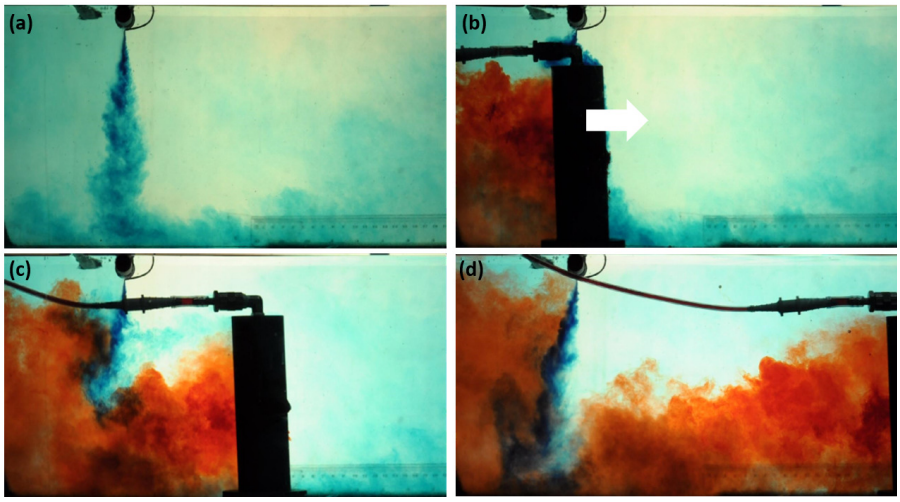

Figure 4: (Colour online) Side views of the interaction between the cylinder and the curtain for $U^* = 0.44$ and $D_m = 0.5$. The cylinder is moving from the dense to the light fluid side (from left to right as marked in (b)). The blue coloured curtain jet separates the dense and the light fluid in (a) and the red dye visualises the cylinder wake and the infiltration. The infiltration across the curtain and the re-establishment process is shown in (c). The curtain is re-established in (d).

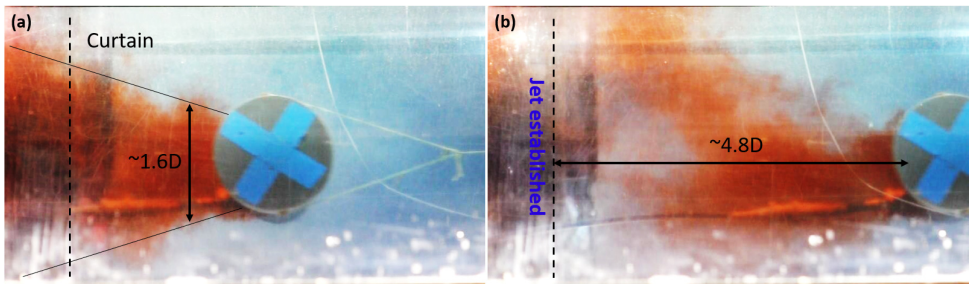

Figure 5: (Colour online) Plan views of the interaction between the cylinder and the curtain for the same parameters as in figure 4, $U^* = 0.44$ and $D_m = 0.5$. The wake expands away from the cylinder and thus the spanwise infiltration across the curtain increases with time. The curtain is re-established in (b). The marked dimensions are in cylinder diameters.

tank, and the reduction in the net transport was very similar for the two values of Q_0. The air curtain itself creates an additional mixing between two sides of the doorway due to the mixing by the jet and impingement at the bottom, and there is some suggestion of increased transport for the stronger curtain.

Furthermore, the reduction of up to 50% suggests that the curtain was re-established before the cylinder reached the end of its traverse. We examine this aspect and other features of the wake–curtain interaction in the next subsection §3.3

3.3. *Dye visualisation and curtain characterisation*

We now present the dye visualisations and use them to explain the observed volume transport and effectiveness measurements. Flow visualisation was conducted for four different

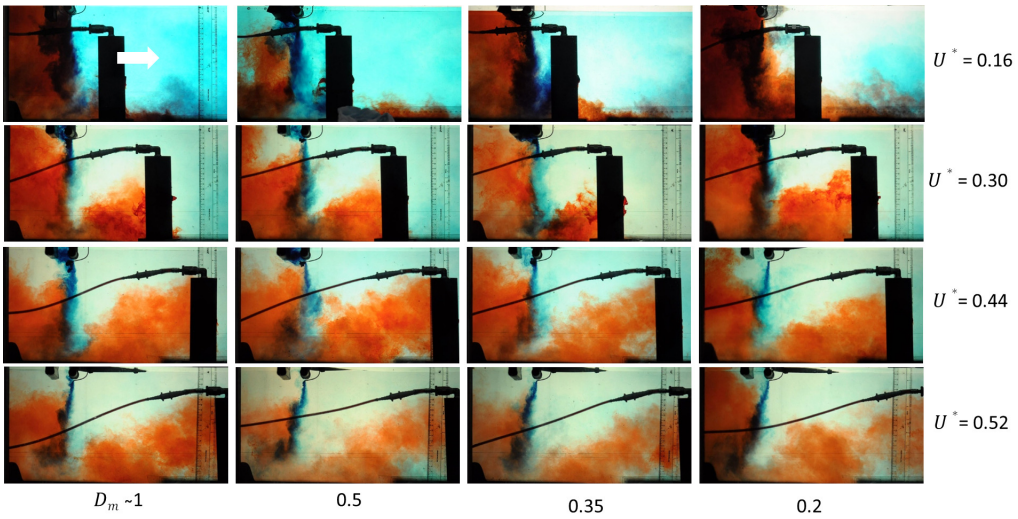

Figure 6: (Colour online) Side views of the cylinder wake and the resulting infiltration when the curtain is first re-established for a range of cylinder speeds and deflection moduli. The cylinder is moving from the dense to the light fluid side and from left to right in the figure as marked by the white arrow.

cylinder speeds and for four different deflection modulus values. The total infiltration is the combined effect of the intruding gravity current and the cylinder wake. However, as mentioned above, since the cylinder wake velocity is an order of magnitude higher than the gravity current speed, we only present the results for the cylinder moving from the dense to the light fluid side of the tank.

Side views of the passage of the cylinder (left to right, marked by the arrow in figure 4(b)) are shown in figure 4. The cylinder was set into motion 0.6 m away from the air curtain which was not influenced by the cylinder at that distance as can be seen in figure 4(a). As the cylinder approached the air curtain, there was a small deflection of the air curtain in the direction of motion of the cylinder. However, the major disruption occurred as the cylinder passed below the air curtain as shown in figure 4(b). Immediately after the cylinder passed through the air curtain, the infiltration of dense (red) fluid into the light fluid side took place during the period of re-establishment of the curtain. At later times, the air curtain re-established by penetrating the wake and the gravity current as seen in figure 4(c). Figure 4(d) illustrates the moment when the air curtain was first re-established. A colour movie *'Movie1'* showing the complete infiltration process can be found in the supplementary material.

Plan views of the interaction for the same parameter values are shown in figure 5. As has already been mentioned, the cylinder has a base with a larger diameter, which obscures the view immediately adjacent to the cylinder. The wake width increases with the distance from the cylinder, so that the span-wise width of the infiltration increased with time. In this case the air curtain is re-established (figure 5(b)) after the cylinder has traveled about 5 cylinder diameters beyond the curtain.

Figure 6 shows the disruption and the re-establishment of the air curtain for different cylinder speeds and values of the deflection modulus. These snapshots show the infiltration when the curtain is first re-established. For a given value of the deflection modulus, the amount of the red dyed fluid on the right hand side of the air curtain increases

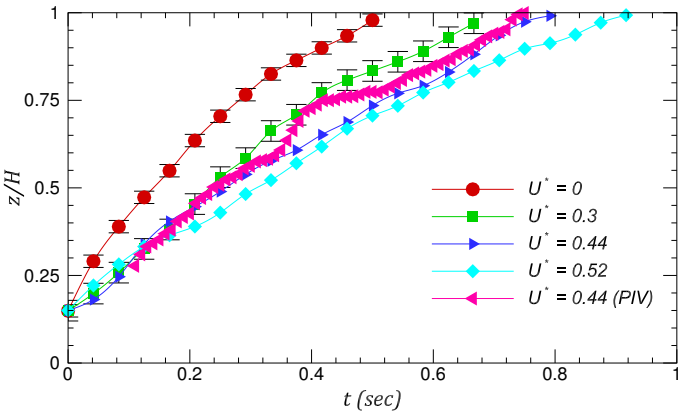

(a) (Colour online) Re-establishment of the curtain as a function of time after the cylinder passage. The front of the curtain is tracked and the time $t = 0$ corresponds to the time when the jet front is at the height of the top of the cylinder, which is $0.15H$ from the nozzle exit. The evolution of the jet is shown for $D_m = 0.5$ and for different cylinder speeds $U^* = 0.3, 0.44, 0.52$.

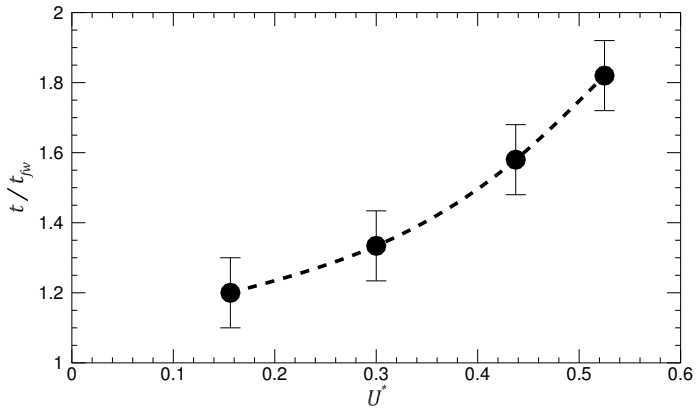

(b) Time taken for the curtain to reach the bottom of the tank for the same experimental parameters as in figure 7a. Here, time is non-dimensionalised by the time t_{fw} taken for the curtain to reach the tank bottom in a quiescent freshwater environment.

Figure 7: The curtain re-establishment characteristics for different cylinder speeds. Lines are shown to describe the trends of the data and also to demarcate among different conditions.

with increasing cylinder speed. However, there is no noticeable influence of the deflection modulus value and, hence, as expected for these parameter values, there is no influence of the gravity current due to the density difference across the doorway on the amount of the infiltrated fluid.

The re-establishment of the air curtain after its disruption determines the total amount of the infiltration by the wake. The dimensionless vertical penetration distance z/H of the jet, measured downwards from the jet nozzle at $z/H = 0$, is plotted as a function of time for different cylinder speeds in figure 7a. The measurements for the case $U^* = 0$ was carried out in the fresh water environment without any density difference. For the

other cylinder speeds, we fixed $D_m = 0.5$. We see that the curtain re-establishment time increased with cylinder speed, presumably a result of the increased momentum in the wake. We will present the detailed results from the PIV in the next subsection. However, here, we briefly present the curtain re-establishment time for $U^* = 0.44$ from the PIV measurements to compare it with dye in figure 7a. The PIV experiment was conducted in the absence of any buoyancy effects. For PIV, we track the curtain front at 100 f.p.s. ($(1/4)^{th}$ of the PIV acquisition rate), whereas the front tracking from dye visualisation is done at 24 f.p.s. In the PIV experiment, the visible bump in the position-time curve is due to the presence of a strong eddy near the curtain front. Apart from that, it is very similar to the dye tracking, which includes the presence of buoyancy. The infiltration time is plotted in figure 7b. The increasing re-establishment time of the air curtain with the increasing cylinder speed is in line with the measured decrease in its effectiveness.

3.4. *Particle Image Velocimetry*

Two-dimensional PIV measurements in a vertical (x-z) plane along the centreline of the channel were first conducted on the planar turbulent jet in the absence of a cylinder wake to validate the base case flow field. For the mean velocity field, we averaged 2500 instantaneous flow fields captured at 400 f.p.s. at two vertical locations below the nozzle. As seen in figure 8(a), the measurements show that the planar jet was fully developed with very little variation in the mean axial velocity $\overline{w}$ at the two downstream locations. The mean axial velocity $\overline{w}$ profile in this plot is normalized by the mean centreline velocity $\overline{w}_c$ at each location and the lateral distance x from the jet axis is normalized by the distance of half velocity point $x_{\frac{1}{2}m}$. For comparison and validation, the data from Gutmark & Wygnanski (1976) and Heskestad (1965) for the planar turbulent jet are also shown in the figure, with reasonable agreement between their data and ours. The axial turbulent intensity w_{rms} profile, scaled by the axial mean velocity $\overline{w}_c$, is plotted against the lateral distance from the jet axis which is also non-dimensionalised by $x_{\frac{1}{2}m}$ in figure 8(b). The present PIV measurements are found to be in reasonable agreement with the hot-wire data of Gutmark & Wygnanski (1976) and Heskestad (1965).

Two-dimensional PIV measurements will now be presented to examine the velocity field in the vertical plane through the axis of the cylinder during the interaction of the air curtain with the cylinder wake. As we saw in § 3.1, the air curtain performance was independent of the direction of the cylinder motion so, as mentioned above, we conducted PIV only for the pure water experiments, series B. The flow was illuminated with a light sheet that passed through the tank base and some of the light sheet was blocked by the cylinder base. In figure 9, this region is blacked out and the cylinder is marked by horizontal lines. The velocity vectors (u, w) in the $x - z$ plane are represented by arrows, and the spanwise component of vorticity $\omega_y = w_x - u_z$ is represented by colours. A video of the PIV is provided in the supplementary material as *'Movie2'*.

In the present case, the curtain was naturally turbulent (figure 8(b)) and, when the cylinder was sufficiently far away from the jet, shear layer eddies were visible on both sides of the jet. As the cylinder approached the air curtain (figure 9(a)), the streamwise velocity induced by the cylinder pushes the jet forward. When the cylinder was closer to the air curtain (figure 9(b)), the central core of the jet was highly perturbed and the shear layer near the cylinder was suppressed.

The air curtain was completely disrupted when the cylinder was underneath it. After the cylinder passage, the air curtain started to re-establish but the wake velocity continued to pull it towards the cylinder (figure 9(c)). The jet trajectory in figures 9(c) and (d) is shown by the white dotted line. The air curtain started to penetrate the cylinder wake from above and, during this time, an unhindered fluid exchange could take place below

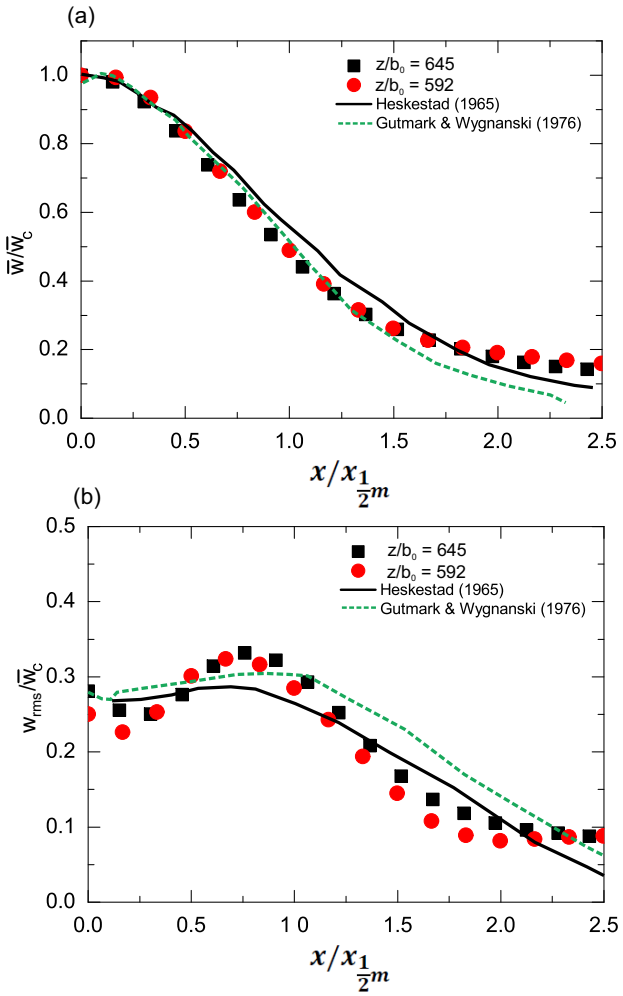

Figure 8: (Colour online) Profiles of the mean and fluctuating vertical (axial) velocity of the turbulent jet produced by the air curtain device in the absence of a cylinder wake measured at two downstream locations $z/b_0 = 592$ and $z/b_0 = 645$. In (a) the profile of the mean axial velocity, normalised by the centreline velocity ($\overline{w}/\overline{w}_c$), is plotted against the normalised lateral distance from the jet axis. In (b), the axial turbulent intensity profile, non-dimensionalised by the mean axial centreline velocity $\overline{w}_c$, is plotted against the normalised lateral distance from the jet axis. For comparison and validation of mean and turbulent properties, the data from Heskestad (1965) and Gutmark & Wygnanski (1976) are also shown, with reasonable agreement between their data and ours.

the region of the re-establishing air curtain (figure 9(c) and 9(d)). As we saw earlier, the air curtain re-establishment after the cylinder passage was slower than in the quiescent tank. This can be interpreted as being due to the cross-flow forcing of the cylinder wake which interferes with the air curtain. The curtain re-establishment behavior such as its temporal evolution and the re-establishment time is very similar for the PIV and dye measurements as already presented in figure 7a.

In figure 10, we present the meandering of the jet during the re-establishment process. The interacting vortex is marked by the dashed red line and the jet trajectory is shown

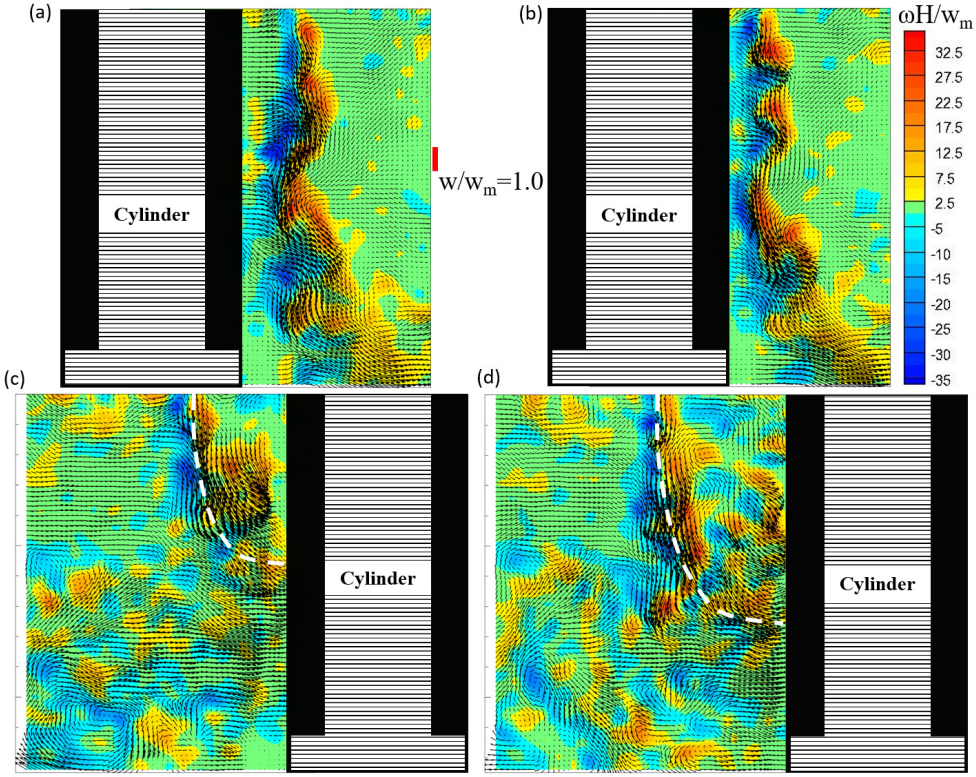

Figure 9: (Colour online) Velocity (arrows) and spanwise vorticity (colours) fields illustrating the passage of the cylinder with speed $U^* = 0.44$ through the air curtain. (a) and (b) shows the distortion of the curtain as the cylinder approaches, and (c) and (d) the flow after the cylinder has passed through the doorway. The black space represents the area where the light is blocked by the cylinder base. The non-dimensional times are (a) $t^* = tw_m/H = -0.69$ and (b) $t^* = tw_m/H = -0.58$. (c) $t^* = tw_m/H = 0.62$ and (d) $t^* = tw_m/H = 0.87$. Similarly to figure 7a, the time $t = 0$ corresponds to the time, when cylinder passes the jet axis. The dimensionless spanwise vorticity ($\omega H/w_m$) is shown beside (b) and the representative length of the velocity vector (w/w_m) is marked beside (a).

by the dashed white line. The induced velocity of the marked vortex is in the clockwise direction in figure 10(a). The jet responds to the velocity induced by these vortical structures and evolves in the direction of the induced velocity. In figure 10(c), a large anti-clockwise vortical structure marked by a magenta ellipse above the establishing jet and a vortex pair marked by the dashed red ellipse can also be observed. The vortex pair induces a strong velocity at the center and the jet is then diverted towards it (figure 10(d)) and the large vortical structure draws it towards the cylinder wake. We have shown in figures 10 the interaction with only two structures whereas, during the re-establishment process, the air curtain interacts in general with many such structures. These are the main cause for the meandering of the jet, which, in turn, produces a higher re-establishment time as seen in figure 7b.

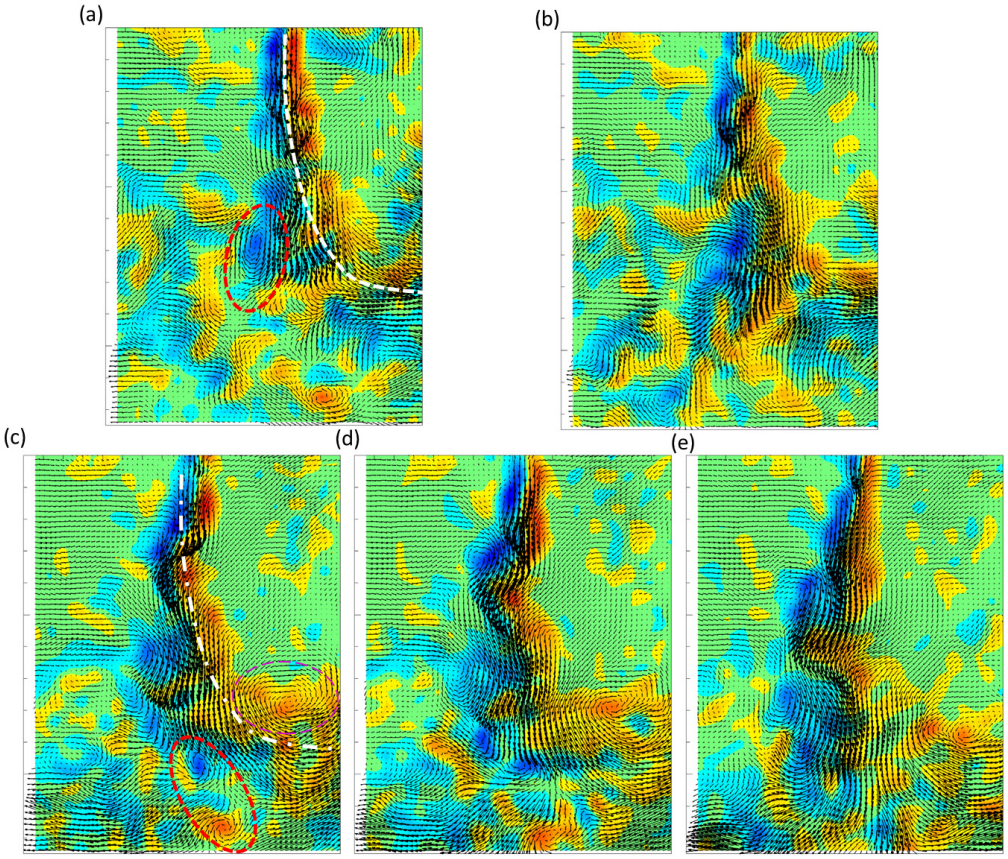

Figure 10: (Colour online) Combined velocity and vorticity fields for a re-establishing curtain after the passage of the cylinder for the same experimental parameters as in figure 9. The white dashed line represents the curtain position. The evolution of the jet is downward and deflected by the cylinder wake as seen in (a). At later times, the jet approaches the tank bottom and is also drawn towards the cylinder. Interaction of the re-establishing jet and the vortex pair is shown further in (c), (d) and (e). The vortex pair is marked by the dashed red line and a single strong vortex by the thin dashed magenta line in (c). The non-dimensional times are (a) $t^* = tw_m/H = 1.10$, (b) $t^* = tw_m/H = 1.26$, (c) $t^* = tw_m/H = 1.95$, (d) $t^* = tw_m/H = 2.04$ and (e) $t^* = tw_m/H = 2.23$.

4. Summary and Conclusions

In the present study, we examined the effect of a cylindrical object, representing a human, passing through the air curtain. Laboratory experiments were conducted using fresh water, salt and sugar solutions, to produce flows dynamically similar to real-scale air curtain installations. We measured the effectiveness of the air curtain with and without the passage of the cylinder, and observed that the effectiveness reduces with increasing cylinder speed. In the absence of traffic we observed that the air curtain can reduce the contaminant transport by up to about 80% with a stable air curtain, while further increase in the curtain momentum reduces its sealing effectiveness. This reduction in performance is related to the extra mixing caused by turbulent jet and stronger impingement at the bottom floor.

The passage of a cylinder reduces the sealing effectiveness and the reduction increases with increasing cylinder speed. The cylinder disrupts the curtain and visualisations of the jet and the cylinder wake show the infiltration of the fluid carried along with the cylinder wake underneath the unestablished jet is the reason for the observed reduction in the effectiveness. With an increasing cylinder speed, the entrainment in the cylinder wake also increases due to the faster wake velocity which induces a longer time for the re-establishment of the curtain. We also observed that the reduction in effectiveness was independent of the travel direction, because of the faster cylinder speed compared to the stack-driven exchange flow in our experiments and as is typical in most practical situations.

We used the time-resolved two-dimensional particle image velocimetry to study the interaction of the jet and the cylinder wake. We observed that the re-establishment process of the jet is highly unsteady and the jet flaps due to the large vortical structures in the wake leading to an increased mixing across the doorway. These nonlinear interactions lead to an increase in establishment time that is faster than linear in the cylinder velocity.

The effect of human passage on the contaminant transport is important in the design and the operation of clean rooms in chemical or pharmaceutical industries and in protecting isolated hospital rooms for infectious and immunocompromised patients from infiltration of air-borne contamination. Our study shows that the human or vehicular traffic reduces the effectiveness and that the volume transported across the curtain increases more than linearly with the traffic speed. To minimize the air curtain disruption, we suggest a slowing down of the traffic just before the air curtain and then the passage across the air curtain with a much reduced velocity. Also, a higher safety factor on D_m will result in a higher jet velocity, which will help in re-establishing the curtain faster and hence result in a lesser entrainment.

5. Supplementary materials

Video caption for supplementary video 1 (Movie1.avi): Temporal evolution of the side view of the interaction using the blue (curtain) and red (cylinder wake) dye for $U^* = 0.44$ and $D_m = 0.5$. The cylinder is moving from the dense to the light fluid side. The video is played at 4.8 times slower than real speed.

Video caption for supplementary video 2 (Movie2.avi): Combined velocity and vorticity field from time resolved PIV measurements of the interaction of the curtain and the cylinder for $U^* = 0.44$ in the absence of any buoyancy effects. The video is played at 16 times slower than real speed. During the cylinder passage, part of the light sheet was blocked by the cylinder base, which can be seen in processed PIV images with mostly zero and few bad velocity vectors in those areas.

Acknowledgement

This research has been supported by the EPSRC through grant EP/K50375/1 and Biddle BV. We would like to thank Prof. Stuart Dalziel and Dr. Jamie Partridge for the discussion and advice during the experiments. We would also like to thank D. Page-Croft for technical support with the experimental setup.

REFERENCES

Adams, N. J., Johnson, D. L. & Lynch, R. A 2011 The effect of pressure differential and care provider movement on airborne infectious isolation room containment effectiveness. *American journal of infection control* **39** (2), 91–97.

Beggs, C. B. 2003 The airborne transmission of infection in hospital buildings: fact or fiction? *Indoor and Built Environment* **12** (1-2), 9–18.

Choi, J. I. & Edwards, J. R. 2012 Large-eddy simulation of human-induced contaminant transport in room compartments. *Indoor air* **22** (1), 77–87.

Costa, J. J., Oliveira, L. A. & Silva, M. C. G. 2006 Energy savings by aerodynamic sealing with a downward-blowing plane air curtain - a numerical approach. *Energy and Buildings* **38**, 1182–1193.

Foster, A. M. 2007 Cfd optimization of air movement through doorways in refrigerated rooms. In *Computational Fluid Dynamics in Food Processing*, pp. 167–193. CRC Press.

Foster, A. M., Swain, M. J., Barrett, R., D'Agaro, P. D. & James, S. J. 2006 Effectiveness and optimum jet velocity for a plane jet air curtain used to restrict cold room infiltration. *International Journal of Refrigeration* **29**, 692–699.

Frank, D. & Linden, P. F. 2015 The effects of an opposing buoyancy force on the performance of an air curtain in the doorway of a building. *Energy and Buildings* **96**, 20–29.

Frank, D. & Linden, P. F. 2014 The effectiveness of an air curtain in the doorway of a ventilated building. *Journal of Fluid Mechanics* **756**, 130–164.

Giráldez, H., Segarra, C. D. Pérez, Rodriguez, I. & Oliva, A. 2013 Improved semi-analytical method for air curtains prediction. *Energy and Buildings* **66**, 258–266.

Gonçalves, J. C., Costa, J. J., Figueiredo, A. R. & Lopes, A. M. G. 2012 CFD modelling of aerodynamic sealing by vertical and horizontal air curtains. *Energy and Buildings* **52**, 153–160.

Gutmark, E. & Wygnanski, I. 1976 The planar turbulent jet. *Journal of Fluid Mechanics* **73** (3), 465–495.

Guyonnaud, L., Solliec, C., de Virel, M. D. & Rey, C. 2000 Design of air curtains used for air confinement in tunnels. *Experiments in Fluids* **28**, 377–384.

Havet, M., Rouaud, O. & Solliec, C. 2003 Experimental investigations of an air curtain device subjected to external perturbations. *International journal of heat and fluid flow* **24** (6), 928–930.

Hayes, F. C. & Stoecker, W. F. 1969*a* Design data for air curtains. *Transactions of the ASHRAE* **75**, 168–180.

Hayes, F. C. & Stoecker, W. F. 1969*b* Heat transfer characteristics of the air curtain. *Transactions of the ASHRAE* **75 (2)**, 153–167.

Heskestad, G. 1965 Hot-wire measurements in a plane turbulent jet. *Journal of Applied Mechanics* **32** (4), 721–734.

Hoffman, P. N., Bennett, A. M. & Scott, G. M. 1999 Controlling airborne infections. *Journal of Hospital Infection* **43**, 203–210.

Howell, R. H. & Shibata, M. 1980 Optimum heat transfer through turbulent recirculated plane air curtains. *Transactions of the ASHRAE* **2567**, 188–200.

Knystautas, R. 1964 The turbulent jet from a series of holes in line. *The Aeronautical Quarterly* **15** (1), 1–28.

Linden, P. F. 1999 The fluid mechanics of natural ventilation. *Annual review of fluid mechanics* **31** (1), 201–238.

Lowbury, E. J. L, Babb, J. R. & Ford, P. M. 1971 Protective isolation in a burns unit: the use of plastic isolators and air curtains. *Journal of Hygiene* **69** (04), 529–546.

Olsthoorn, J. & Dalziel, S. B. 2015 Vortex-ring-induced stratified mixing. *Journal of Fluid Mechanics* **781**, 113–126.

Rajaratnam, N. 1976 *Turbulent jets*, , vol. 5. Elsevier.

Rouaud, O. & Havet, M. 2006 Behavior of an air curtain subjected to transversal pressure variations. *Journal of environmental engineering* **132** (2), 263–270.

Sirén, K. 2003*a* Technical dimensioning of a vertically upwards blowing air curtain - part i. *Energy and Buildings* **35**, 681–695.

Sirén, K. 2003*b* Technical dimensioning of a vertically upwards blowing air curtain - part ii. *Energy and Buildings* **35**, 697–705.

Tang, J. W., Nicolle, A., Pantelic, J., Klettner, C. A., Su, R., Kalliomaki, P., Saarinen, P., Koskela, H., Reijula, K., Mustakallio, P. & Cheong, D. K. 2013 Different types of door-opening motions as contributing factors to containment failures in hospital isolation rooms. *PloS one* **8** (6), e66663.